

Wetening of the Southern Hemisphere Land Monsoon during 1901–2014

JIAN CAO^{a,b}, XUANQIANG LIAN,^a MIN CAO,^c BIN WANG,^{b,d} HAO WANG,^a XIAOWEI ZHU,^e AND HAIKUN ZHAO^a

^a Key Laboratory of Meteorological Disaster, Ministry of Education, Joint International Research Laboratory of Climate and Environment Change, Collaborative Innovation Center on Forecast and Evaluation of Meteorological Disasters, Nanjing University of Information Science and Technology, Nanjing, China

^b Earth System Modeling Center, Nanjing University of Information Science and Technology, Nanjing, China

^c School of Business, Nanjing University of Information Science and Technology, Nanjing, China

^d Department of Atmospheric Sciences, University of Hawai'i at Mānoa, Honolulu, Hawaii

^e Ningxia Climate Center, Ningxia, China

(Manuscript received 8 February 2023, in final form 21 September 2023, accepted 25 September 2023)

ABSTRACT: The causes of historical changes in the Southern Hemisphere (SH) monsoon are less understood than the Northern Hemisphere (NH) counterpart. Unlike the decline in the NH monsoon during 1901–2014, we found that the SH land monsoon precipitation significantly increased during 1901–2014 in observation, reanalysis, and most historical simulations from phase 6 of the Coupled Model Intercomparison Project (CMIP6). The observed increase in SH land monsoon precipitation is dominated by the Australian and South American monsoons. Moisture budget analysis suggests that half of the wettening is attributable to the strengthening of monsoon circulation, and only one-fifth is caused by atmospheric moistening. The SH monsoon circulation change is mainly affected by the sea surface temperature (SST) gradient between the Indo-Pacific and the eastern Pacific. It enhances the tropical zonal circulation that redistributes the moisture from tropical oceans to land monsoon regions by strengthening the lower-tropospheric convergence and convection. The CMIP6 models, which successfully reproduced the SST contrast between the Indo-Pacific and eastern Pacific, simulate the wettening of the SH monsoon during the historical period; otherwise, the SH monsoon is weakened. In a meridional sense, reanalysis and CMIP6 simulations both demonstrated that the strengthening of SH monsoon convection plays a vital role in the long-term change of zonal mean Hadley circulation, albeit the monsoon band only accounts for 1/3 of the global longitudinal area. Results from this study are useful for constraining the future projection of SH monsoon and understanding the long-term change of Hadley circulation.


KEYWORDS: Southern Hemisphere; Hadley circulation; Walker circulation; Monsoons; Climate change

1. Introduction

The SH and the NH monsoons are two components of the global monsoon system, which are fundamentally driven by the annual cycle of solar radiation and represent the global tropical atmosphere overturning by mass, momentum, and energy (Trenberth et al. 2000; Bordoni and Schneider 2008; Wang et al. 2014; An et al. 2015). Precipitation of the SH monsoon is the lifeblood of agriculture and hydropower sectors in southern developing countries where climate resilience is relatively low. Prior studies often analyzed the NH and SH monsoons in parallel. Results suggest an in-phase change during some climate conditions but an out-of-phase change during others, although they are forced by the same external forcing and simulated by the same group of coupled models (Wang et al. 2006; Cheng et al. 2012; Hsu et al. 2012; Lee and Wang 2014; Jiang et al. 2015; Yan et al. 2016; Cao et al. 2019b; D'Agostino et al. 2019, 2020; Scussolini et al. 2019; Cao and Zhao 2020; Wang et al. 2020; Cao et al. 2020, 2022). This suggests that NH and SH monsoons may be driven by distinct

physical processes (Liu et al. 2012; Brown et al. 2016; Jin et al. 2020); thus, the mechanisms responsible for the SH counterpart need to be better understood. To faithfully project the future SH monsoon, there is a need to improve the driving mechanism of long-term change of past and historical SH monsoons.

Under the wet-get-wetter paradigm, the warming of the global climate is expected to increase the precipitation over climatological wet regions, as in monsoon regions (Held and Soden 2006; Wang et al. 2012). Proxy data and paleoclimate simulations revealed that the NH monsoon is indeed wettening (Jiang et al. 2015; D'Agostino et al. 2019; Scussolini et al. 2019; Cao et al. 2021), but the SH monsoon dries (Jiang et al. 2015; Scussolini et al. 2019; D'Agostino et al. 2020) during the last interglacial and mid-Holocene warm periods. During the last glacial maximum period, both NH and SH monsoons were drier than the present, although the magnitudes of precipitation reduction show different sensitivity in the NH and SH monsoons (Yan et al. 2016; Cao et al. 2019a,b). Since the last glacial maximum, it has been found that the NH and SH monsoons have a significant antiphase relationship on the millennium time scale (Cheng et al. 2012; Li et al. 2022). Moreover, the NH and SH monsoons have shown a similar pace on the centennial time scale in the most recent 1000 years, although the NH and SH monsoons are affected by different physical processes (Liu et al. 2009, 2012).

 Denotes content that is immediately available upon publication as open access.

Corresponding authors: Jian Cao, jianc@nuist.edu.cn; Bin Wang, wangbin@hawaii.edu

DOI: 10.1175/JCLI-D-23-0066.1

© 2023 American Meteorological Society. This published article is licensed under the terms of the default AMS reuse license. For information regarding reuse of this content and general copyright information, consult the AMS Copyright Policy (www.ametsoc.org/PUBSReuseLicenses).

On the other hand, the CMIP models projected different trends in NH and SH monsoon precipitation under anthropogenic global warming. There are explained from the perspectives of atmospheric circulation and energetic framework (Hsu et al. 2013; Lee and Wang 2014; Cao et al. 2020; Wang et al. 2020; Ha et al. 2020; D'Agostino et al. 2019, 2020). A wetter future NH monsoon is often found in CMIP5/6 projection, but consensus on how SH monsoons will change is still low (Lee and Wang 2014; Cao et al. 2020; Wang et al. 2020; Chen et al. 2020), albeit the large intermodel spread of SH monsoons could be understood by the uncertainty in monsoon circulation change (Cao et al. 2020) and net atmospheric energy input (D'Agostino et al. 2020). The middle-of-the-road scenarios in CMIP5 and CMIP6 both projected an insignificant change in the SH monsoon, while it tended to be wet under higher emission scenarios (Chen et al. 2020). The increase in projected NH monsoon precipitation is often explained by the compelling effect of atmospheric moistening under global warming and the weakening of monsoon convergence (Hsu et al. 2013; Endo and Kitoh 2014; Wang et al. 2020). However, the changes in SH monsoons are relatively less investigated. The low confidence of projected SH monsoon may be due to the poorly understood SH monsoon system responses to anthropogenic and/or natural forcing-driven climate change and, on the other hand, due to the defectiveness of model physics in the climate models (Cao et al. 2020; Zhou et al. 2020b).

The observation and reanalysis dataset from the instrumental period provided opportunities to explore the long-term change of the NH/SH monsoon and its associated mechanisms. Studies revealed various NH monsoon precipitation trends with different lengths of analysis periods. Monsoon precipitation decreased during the 1950s–1980s and increased afterward (Wang et al. 2018; Huang et al. 2019; Monerie et al. 2022). An overall decrease in monsoon precipitation is detected and attributable to the anthropogenic aerosols (Bollasina et al. 2011; Polson et al. 2014; Zhou et al. 2020a; Monerie et al. 2022) and the multidecadal oscillation of tropical SSTs (Wang et al. 2018; Zhang et al. 2018). Recently, Cao et al. (2022) found a significant decrease in the NH monsoon precipitation during the historical warming period (1901–2014). This drying is attributed to the higher sensitivity of NH monsoons to anthropogenic aerosol than greenhouse gases, although the latter dominates Earth's warming. The aerosols' efficacy in monsoon precipitation is 5 times that of greenhouse gases, mainly attributed to the higher sensitivity of monsoon circulation and surface evaporation to aerosols. However, the long-term change of SH monsoon is still relatively unknown. It is uncertain whether the SH monsoon is also drying and dominated by the higher sensitivity from the aerosol. Previous studies investigated the SH monsoon changes in relatively short periods, showing different trends. There is no significant change in SH monsoon during the latter half of the last century (e.g., the 1950s–2000s) (Wang and Ding 2006; Zhou et al. 2008), whereas its trend has become positive when considering the recent few decades (e.g., 1979–2011) (Wang et al. 2012; Lin et al. 2014). Both periods may be significantly influenced by the Earth system's internal modes, although the effect of external forcing may be detected over some regions (Wang et al. 2018; Ha et al. 2020). Zhang and Zhou (2011) examined the linear trend of SH

monsoon precipitation during 1901–2001, which showed an increase. However, its driving mechanism is unknown.

The variation of long-term change of SH monsoon is often linked to the zonal mean location of the intertropical convergence zone (ITCZ) and Hadley circulation (Charney 1969; T. Schneider et al. 2014; Boos and Korty 2016; Biasutti et al. 2018; Gadgil 2018). According to the energetic framework, the Hadley cell moves to the warmer hemisphere in order to balance the cross-equatorial heat transport from the ocean. Thus, the ITCZ, which is collocated with the ascending branch of the Hadley cell, shifts to the more energetic hemisphere (Broccoli et al. 2006; Donohoe et al. 2013; Frierson et al. 2013; Bischoff and Schneider 2014; Xiang et al. 2018; Biasutti et al. 2018). This is broadly consistent with the increase of monsoon precipitation when the ITCZ migrates poleward, supporting the view of monsoons as a local expression of the ITCZ (T. Schneider et al. 2014; Biasutti et al. 2018; Gadgil 2018). It has been challenged by other perspectives, including the following: 1) Theoretically, the monsoons are characterized by angular momentum conserving circulations, differing from the view of ITCZ, which is strongly influenced by momentum fluxes associated with large-scale transient eddies (Biasutti et al. 2018; Geen et al. 2020). 2) Also, a large portion of the ITCZ is embedded in the monsoon regions; thus, the annual migration of ITCZ is largely influenced by the monsoon system (Wang et al. 2014, 2017). Therefore, the relationship between the monsoon and Hadley cell/ITCZ is still inconclusive.

In this study, we explore the trends of the SH monsoon during 1901–2014 from observation, reanalysis, and CMIP6 historical simulations. We only focus on the land area where longer observational datasets exist. We found the consistent wettening of SH monsoon in the three types of datasets. The analysis demonstrates the roles of atmospheric moisture and monsoon circulation on the long-term change in SH monsoon. The trends in the two processes are attributed to the influence of global warming and the SST gradient over the tropics, respectively. In addition, the dominance of monsoonal meridional circulation to the zonal mean Hadley cell is discussed. In the next section, the data and methods are introduced. Section 3 analyzes the long-term trend of SH monsoon in observation and reanalysis and verified the SST gradient hypothesis in the reanalysis, and they are proved by the CMIP6 historical simulations. The conclusions are provided in the last section.

2. Data and method

a. Observation, reanalysis, and simulation data

Three monthly global land observational precipitation datasets are used to reveal the long-term change of the SH monsoon during the historical period: 1) Version 7 of the Global Precipitation Climatology Centre (GPCC) covers the period of 1900–2016 with a resolution of $0.5^\circ \times 0.5^\circ$ (U. Schneider et al. 2014); 2) version 4.04 of the Climate Research Unit (CRU) covers 1900–2020 with a resolution of $0.5^\circ \times 0.5^\circ$ (Harris et al. 2014), and 3) version 4.01 of the University of Delaware (UDEL) covers 1900–2017 with a resolution of $0.5^\circ \times 0.5^\circ$ (Willmott and Matsuura 2001). The average of the three observational datasets

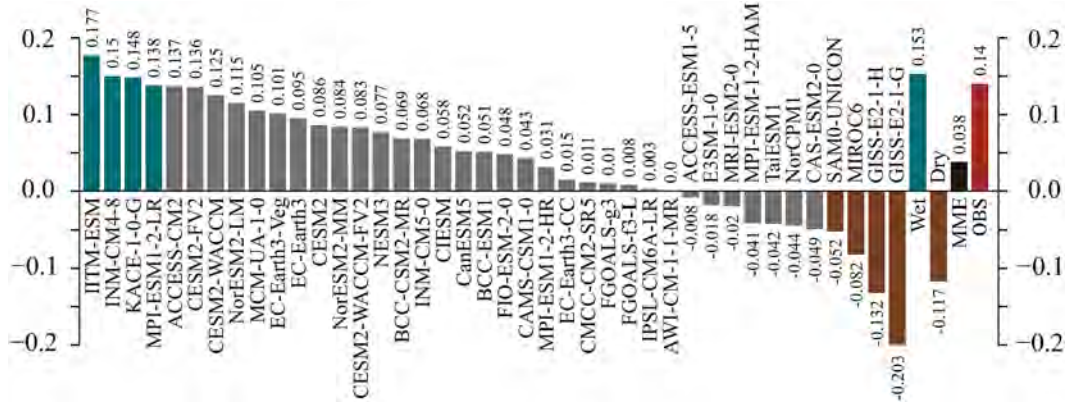


FIG. 1. Linear trends ($\text{mm day}^{-1} \text{ century}^{-1}$) of SH monsoon precipitation in the historical experiment (1851–2014) of 40 CMIP6 models. The four models with the largest drying and wetting trends are marked by green and brown colors, respectively. “Wet” and “Dry” indicate the ensemble mean of the four models with the largest drying and wetting trends, respectively. MME is the ensemble mean of the 40 CMIP6 models.

is used as the OBS to define the monsoon domain and to examine the monsoon precipitation change. Four sets of reanalysis datasets are used to confirm the long-term trend of SH monsoon and understand its physical processes: 1) The Twentieth Century Reanalysis Project data from the National Oceanic and Atmospheric Administration for 1836–2015 (NOAA-20C; Compo et al. 2011), 2) the European Centre for Medium-Range Weather Forecasts (ECMWF) reanalysis of the twentieth century during 1900–2010 (ERA-20C; Poli et al. 2016), 3) the National Centers for Environmental Prediction (NCEP)–National Center for Atmospheric Research (NCAR) reanalysis dataset during 1948–2021 (NCEP1; Kalnay et al. 1996), and 4) the Japanese 55-year Reanalysis Project for 1958–2021 (JRA-55; Kobayashi et al. 2015). The sea surface temperature (SST) used in this study is from the Met Office Hadley Centre (Rayner et al. 2003), which is the major source of surface temperature assimilation for NOAA-20C and ERA-20C dataset (Compo et al. 2011; Poli et al. 2016). The monthly mean precipitation, evaporation, three-dimensional winds, sea level pressure, and geopotential height are used. All reanalysis data are interpolated to a uniform resolution of $2^\circ \times 2^\circ$ to facilitate comparison. We focus on the austral summer [December–March (DJFM)] during the period of 1901–2014 since it is the common period among observation, reanalysis, and CMIP6 historical simulations.

We verified the ability of the coupled model to simulate the long-term change in SH monsoon using the historical simulations from 40 CMIP6 models (Eyring et al. 2016). One realization from each model’s historical simulation is used. Figure 1 introduces the models and the linear trends of the SH monsoon precipitation in the individual model. The historical simulation is forced by observed nature and anthropogenic forcings from 1850 to 2014. The monthly mean precipitation, three-dimensional winds, and surface temperature data are used with the interpolated resolution of $2^\circ \times 2^\circ$.

b. Methods

Following prior studies, the SH land monsoon domain is defined as the regions with the precipitation annual range larger

than 2.5 mm day^{-1} and summer precipitation exceeding 50% of the annual total (Wang et al. 2012; Cao et al. 2022). The annual range is the difference between austral summer (DJFM) and winter [June–September (JJAS)]. The recent 30 years of the OBS data are used to define the monsoon domain (red curves in Fig. 2). Thus, we only examine the land monsoon precipitation change in this study. The defined SH monsoon region includes the South African monsoon (SAF), Australian monsoon (AUS), and South American monsoon (SAM) regions.

Moisture budget analysis is often employed to understand the determining factors for the changes in monsoon precipitation (Chou et al. 2009; Seager et al. 2010; Chadwick et al. 2013). The moisture conservation equation in pressure coordinates for precipitation could be expressed as

$$P' \approx E' - \partial_t \langle q \rangle' - \langle V_h \cdot \nabla_h q \rangle' - \langle \omega \partial_p q \rangle', \quad (1)$$

where P represents the precipitation, E represents evaporation, q denotes the specific humidity, \mathbf{V} is the three-dimensional wind vector, and ∂_t is the time derivative. Angle brackets ($\langle \rangle$) denote the integration from the surface to 100 hPa, and primes ($'$) denote the linear trend. For seasonal mean motion, the local rate of change ($\partial_t \langle q \rangle'$) can be neglected. The term $-\langle V_h \cdot \nabla_h q \rangle'$ represents horizontal advection of horizontal moisture gradient. The term $-\langle \omega \partial_p q \rangle'$ represents vertical moisture advection, which can be divided as

$$-\langle \omega \partial_p q \rangle' = -\langle \overline{\omega \partial_p q} \rangle' - \langle \omega' \partial_p \overline{q} \rangle' - \text{NL}. \quad (2)$$

Since $-\langle V_h \cdot \nabla_h q \rangle'$ and NL are both small terms, they can be omitted. Therefore, the changes in precipitation can be expressed as

$$P' \approx E' - \langle \overline{\omega \partial_p q} \rangle' - \langle \omega' \partial_p \overline{q} \rangle'. \quad (3)$$

In Eq. (3), $-\langle \overline{\omega \partial_p q} \rangle'$ and $-\langle \omega' \partial_p \overline{q} \rangle'$ are the precipitation change due to atmospheric moisture change (moisture effect) and circulation change (circulation effect), respectively (Wang et al. 2020).

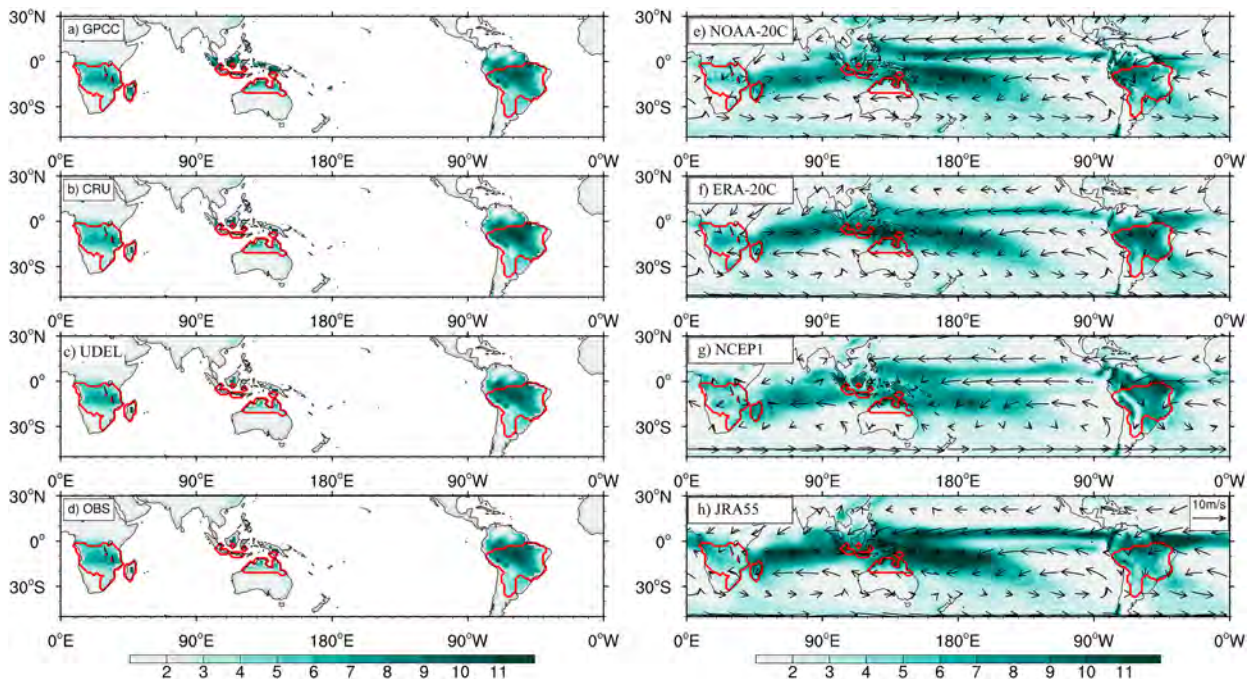


FIG. 2. Climatology of austral summer (DJFM) precipitation (mm day^{-1}) and 850-hPa circulation (m s^{-1}) for the period of 1985–2014, for (left) observation and (right) reanalysis: (a) GPCC, (b) CRU, (c) UDEL, (d) the average of (a)–(c) as OBS, (e) NOAA-20C, (f) ERA-20C, (g) NCEP1, and (h) JRA-55. The red curves outline the SH monsoon region.

In this study, we used Sen's slope and the Mann–Kendall test to obtain the long-term trend and its statistical significance (Kendall 1955).

3. Wettening of SH monsoon since 1901 in observation and reanalysis

a. Climatology and trends of SH monsoon

The precipitation climatologies from observations and reanalysis are shown in Fig. 2 for austral summer (DJFM) during 1985–2014. In the austral summer, intensive precipitation occurs in the SH monsoon regions (Fig. 2). The GPCC, CRU, and UDEL data consistently show that the majority of precipitation happens in the monsoon region with precipitation intensity peak near 10°S . Due to the high similarity of the three datasets, it is reasonable to use their average as OBS (Fig. 2d). As shown in Figs. 2e–h, the four reanalysis datasets all reasonably captured the spatial distribution of the monsoon precipitation as in the OBS. In terms of the monsoon circulation, the SAF monsoon circulation is characterized by the convergence of northeasterly trade winds from the north Indian Ocean, southwest winds from the Atlantic Ocean, and southeast winds from the south Indian Ocean; the AUS monsoon is located in the convergence zone of westerly wind from tropical Indian Ocean and easterly wind from the South Pacific Ocean; the SAM monsoon is in the region of the South Atlantic convergence zone (Figs. 2e–h).

Figure 3 shows the spatial pattern of long-term trends of austral summer (DJFM) precipitation from observation and

reanalysis data during 1901–2014, except for ERA-20C during 1901–2010, NCEP1 during 1948–2014, and JRA-55 during 1958–2014. The observational data, including GPCC, CRU, and UDEL, have a similar pattern of precipitation trend over the land monsoon region (figure not shown). Overall, the OBS shows a wettening over the northeastern SAF and a drying over the rest of the southern African continent (Fig. 3a). Over the AUS region, the trend is dominated by increased precipitation. Over the SAM, precipitation is strengthened over the northwest of Brazil, Bolivia, Paraguay, and the northern part of Argentina, and drying is over eastern Brazil (Fig. 3a). The trend pattern is broadly consistent with that since the 1950s, as investigated by Zhou et al. (2020a). Although the starting years of the linear trends are different in the reanalysis datasets, all of them generally showed an increase in monsoon precipitation over AUS, the majority of SAM, and parts of the southern African continent (Figs. 3b–d). The consistency is relatively low over the SAF due to the different trend patterns in the different reanalysis datasets (Alexander et al. 2020). The NOAA-20C and ERA-20C both have a dipole pattern of precipitation over the SAF continent, while the polarity is opposite. Although the linear trends are calculated starting from 1948 to 1958 for the NCEP1 and JRA-55 datasets, respectively, they both showed wettening over the northern SAF and drying over the southern SAF (Figs. 3b–d). Interestingly, all reanalysis datasets show an increase in precipitation over eastern Brazil; it is not supported by the observation (Fig. 3). The observed increase in precipitation is over the southern SAM, while the consistency is relatively low among the reanalysis datasets. It is also noted by Alexander et al. (2020)

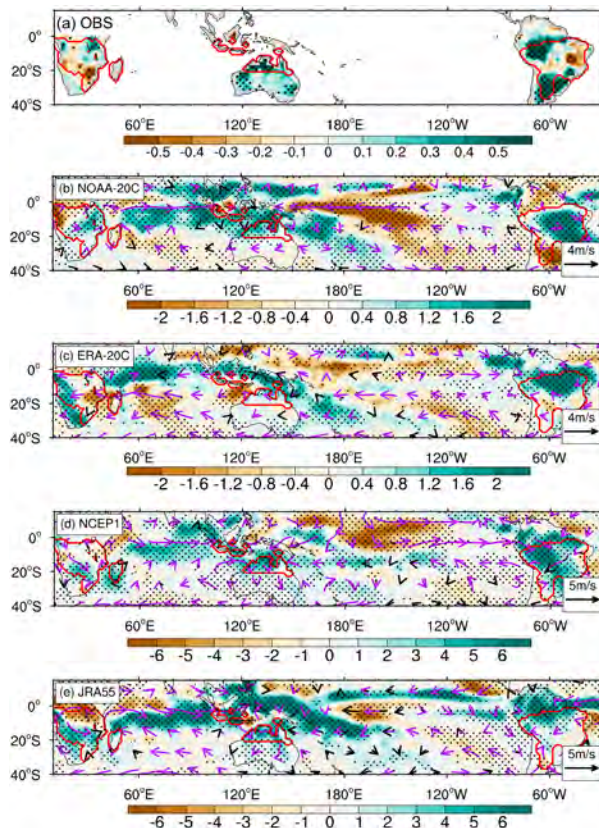


FIG. 3. Sen's trends of precipitation ($\text{mm day}^{-1} \text{ century}^{-1}$) and 850-hPa circulation ($\text{m s}^{-1} \text{ century}^{-1}$) during austral summer (DJFM) for observation and reanalysis, for (a) OBS (the average of GPCC, CRU, and UDEL) during 1901–2014, (b) NOAA-20C during 1901–2014, (c) ERA-20C during 1901–2010, (d) NCEP1 during 1949–2014, and (e) JRA-55 during 1959–2014. The red curves outline the SH monsoon region. Dots represent the trends of precipitation significant at a 90% confidence level. Purple vectors represent the trends of circulation significant at a 90% confidence level.

that considerable uncertainty of tropical land precipitation exists in reanalysis datasets.

In addition, the trends of tropical precipitation in reanalysis data show consistent wettening over the equatorial Indian Ocean and Maritime Continent and drying over the equatorial central Pacific Ocean (Figs. 3b–d). The linear trends of 850-hPa circulation convergence are consistent with the precipitation, showing one couplet of westerly wind over the tropical Indian Ocean and easterly wind over the tropical central and western Pacific Ocean and another couplet of westerly wind over the tropical eastern Pacific and easterly wind over the tropical Atlantic Ocean (Figs. 3b–d). The winds converge over the Maritime Continent and SAM and diverge over the central Pacific Ocean. The anomalous circulation could cause the change of boundary moisture advection and convergence, leading to the anomalous tropical precipitation pattern and monsoon precipitation.

To quantitatively assess the long-term change in the SH monsoon, we averaged the precipitation over the SH land

monsoon region. This is a more convenient method to study the monsoon precipitation change on a hemispheric scale, as in many previous studies (Wang and Ding 2006; Zhang and Zhou 2011). The time series of the precipitation from the whole SH monsoon and each region, relative to their climatological mean, for both observation and reanalysis, are shown in Fig. 4. The evolution of precipitation anomalies from the OBS and reanalysis datasets all suggest wettening of SH monsoons (Figs. 4a,e). The OBS has an increasing trend of $+0.14 \text{ mm day}^{-1} \text{ century}^{-1}$ during 1901–2014, exceeding a 95% confidence level by the Mann–Kendall test. Four reanalysis datasets all confirmed the long-term wettening of SH monsoon, especially in the longer datasets from the NOAA-20C and ERA-20C. The NOAA-20C and ERA-20C have similar trends of $+0.73$ and $+0.62 \text{ mm day}^{-1} \text{ century}^{-1}$, respectively, although the magnitudes are both larger than the observation. The relatively short length of reanalysis of NCEP1 and JRA-55 yields larger wetting trends from the 1950s to 2014. The overestimation of precipitation trends in the reanalysis may be caused by the shortage and lower reliability of the observations for data assimilation in the early part of the twentieth century (Compo et al. 2011; Poli et al. 2016; Marshall 2003).

On regional scales, the linear trends of SAF, AUS, and SAM precipitation are separately investigated (Fig. 4). In the OBS, the monsoon precipitation increased over the AUS and SAM, but the SAF monsoon has a drying trend (Figs. 4b–d). The SAF precipitation has an insignificant trend of $-0.019 \text{ mm day}^{-1} \text{ century}^{-1}$. The increases in AUS and SAM monsoon precipitation are $+0.15$ and $0.24 \text{ mm day}^{-1} \text{ century}^{-1}$, respectively. Both are statistically significant at a 99% confidence level. The NOAA-20C and ERA-20C datasets both reproduced the wettening of monsoons over the AUS and SAM (Fig. 4), and NOAA-20C has significant positive trends ($p < 0.01$) over the AUS and SAM. Both reanalysis datasets have an insignificant change in SAF precipitation. The magnitudes of the positive trends are comparable in the two reanalysis datasets over both AUS and SAM regions, although both are overestimated compared to the OBS (Fig. 4). The linear trends of regional monsoon precipitation have a larger magnitude in the NCEP1 and JRA-55 than in the two twentieth-century analysis datasets. In general, the reanalysis data could reproduce the observed wetting trend of SH monsoons on hemispheric and regional scales (over AUS and SAM) since 1901, although the magnitudes are overestimated. In the two relatively longer-length reanalysis datasets, the significance of wettening is more consistent with the OBS. In the next section, we will only focus on the NOAA-20C reanalysis to explore the physical mechanisms responsible for the wettening of SH monsoon. Compared to the ERA-20C, the NOAA-20C is more reasonably assimilated the SH observations, and it is the mean of 56-member ensemble simulations (Compo et al. 2011).

b. Mechanisms responsible for the wettening of SH monsoon

The moisture budget analysis facilitates understanding the relative role of evaporation, atmospheric moistening, and monsoon circulation convergence on precipitation change.

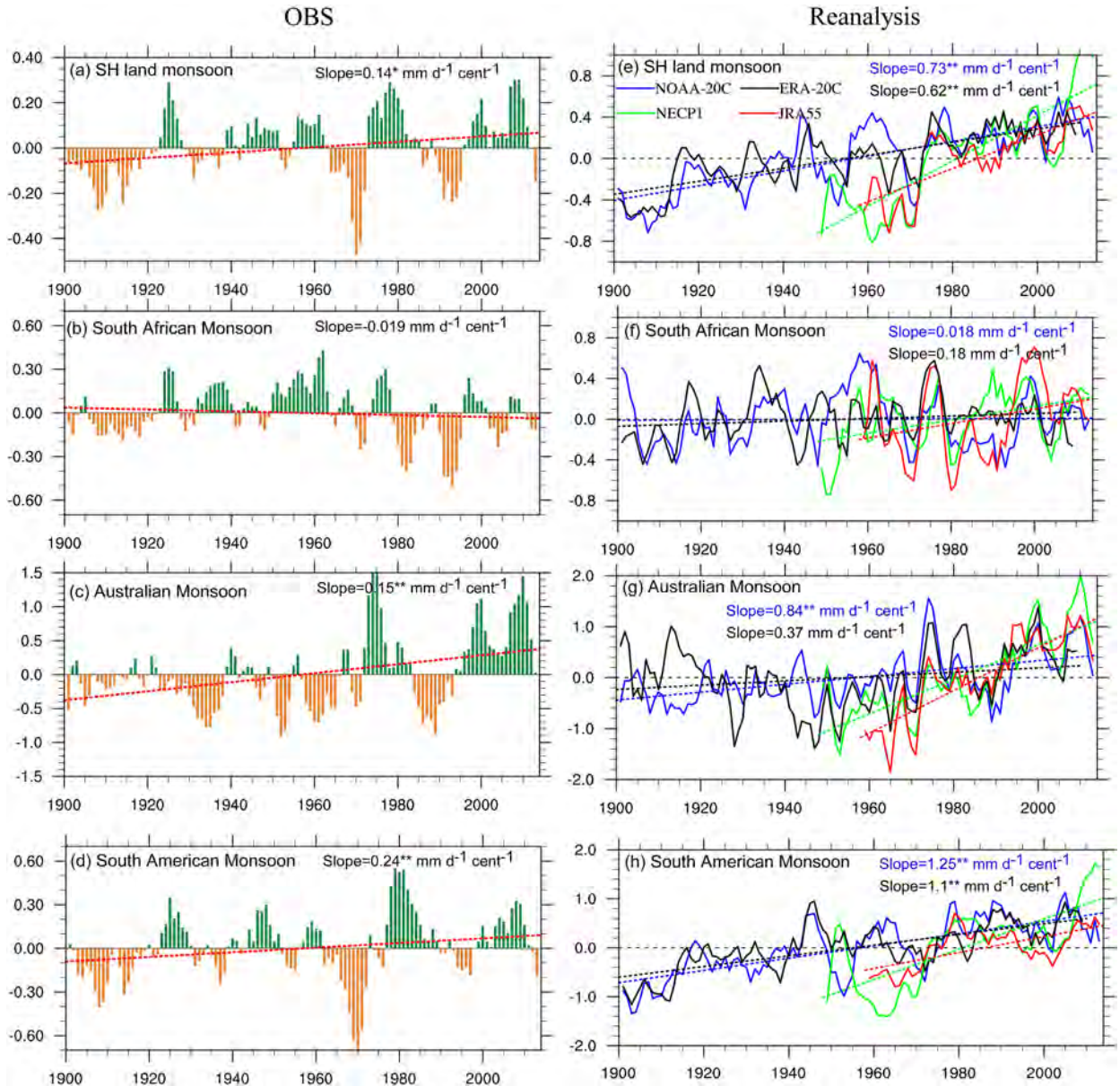


FIG. 4. Changes of SH monsoon precipitation anomalies and three regional monsoon precipitation (mm day^{-1}) from (left) observation and (right) four reanalysis datasets for (a),(e) SH monsoon precipitation, (b),(f) SAF precipitation, (c),(g) AUS precipitation, and (d),(h) SAM precipitation. The bars in (a) and solid curves in (b) indicate the 3-yr running-mean SH monsoon precipitation. The dashed lines indicate linear trends. One and two asterisks (*) and (**) indicate the trend significant at 95% and 99% confidence levels, respectively.

The warming of Earth's temperature increases the atmospheric moisture capability; thus, it potentially enhances precipitation without a change in monsoon circulation. This is typically termed the moisture effect ($-\langle \overline{\omega} \partial_p q' \rangle$), although it is mainly due to uniform global warming and climatological circulation (Wang et al. 2020). The heterogeneous global warming generates thermal contrasts on global and regional scales. They alter the atmospheric circulation and its associated moisture transport. This process is named the dynamic effect in previous studies (Hsu et al. 2013; Zhang and Zhou 2011),

while it is termed the circulation term here ($-\langle \omega' \partial_p \bar{q} \rangle$). Based on Eq. (3), the evolution and long-term trends of SH monsoon precipitation and its components, including evaporation, moisture term, and circulation term, from NOAA-20C are shown in Fig. 5. Evaporation has a small positive impact on monsoon precipitation increase (Fig. 5a). The increase of atmospheric moisture associated with global warming enhances the SH monsoon with a rate of $+0.16 \text{ mm day}^{-1} \text{ century}^{-1}$, while it is not the dominant contributor, only accounting for $\sim 21\%$ of the total increase ($+0.73 \text{ mm day}^{-1} \text{ century}^{-1}$). The

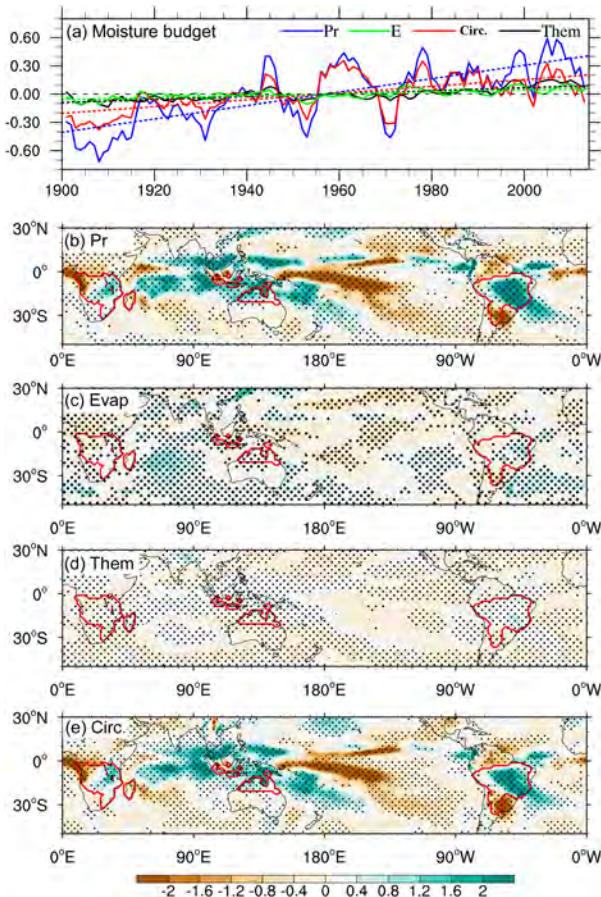


FIG. 5. Moisture budget analysis for the SH monsoon precipitation change for 1901–2014. (a) Moisture budget terms over the SH monsoon region (mm day^{-1}), and linear trends ($\text{mm day}^{-1} \text{ century}^{-1}$) for (b) precipitation, (c) evaporation, (d) thermodynamic term, and (e) circulation term. Dots represent the trends of precipitation significant at a 90% confidence level.

wetting of the SH monsoon is largely explained by the circulation term, which is from the enhancement of monsoon circulation (Fig. 5a). It has a trend of $+0.38 \text{ mm day}^{-1} \text{ century}^{-1}$, accounting for $\sim 51\%$ of the total increase ($+0.73 \text{ mm day}^{-1} \text{ century}^{-1}$). Interestingly, the interannual to decadal variation of monsoon precipitation is also highly correlated with the circulation term, suggesting the importance of monsoon circulation on interannual to decadal monsoon precipitation change. The correlation coefficient between the circulation term and SH monsoon precipitation is 0.95 after removing the linear trend, significant at a 99% confidence level (Fig. 5a). It suggests that the monsoon circulation change is fundamental for interannual to centennial variation of monsoon precipitation over the SH.

Comparing the spatial pattern of the linear trends for precipitation and circulation effect shows that the two patterns are similar, and the magnitudes are comparable over the monsoon region and the tropics (Figs. 5b,e). That means the circulation change has a critical role in shaping the tropical precipitation change on the centennial scale in NOAA-20C. The circulation

change causes an increase in moisture convergence over the Indo-Pacific sector and SAM region and a decrease in moisture over the central Pacific and eastern Atlantic (Fig. 5e). This zonal quadrupole-like pattern may suggest the critical role of Walker circulation change. The contribution from evaporation and moisture effect is weaker than the circulation effect.

What has caused the increase in moisture and circulation effects during 1901–2014? The linear trend of SST shows the warming of the global surface with some spatial features. It increases the boundary layer moisture, especially over the monsoon regions (Fig. 6a). The moistening of the lower troposphere contributed to the increase of the moisture term; thus, it has a positive contribution to the increase of SH monsoon (Fig. 6a). In terms of the spatial pattern of SST change, there is larger warming over the Indo-Pacific region and the South Atlantic Ocean and less warming over the eastern Pacific Ocean (Fig. 6a). This SST pattern increases the sea level pressure over the less-warmed eastern Pacific Ocean and lowers the sea level pressure over the Maritime Continent. The surface pressure gradient drives the circulation; thus, the response of lower-tropospheric circulation is characterized by the easterly and westerly anomalies on the climatological ascending branch of the Walker circulation (Fig. 6). The midlevel ascending and descending is enhanced over the tropical Indo-Pacific Ocean and tropical central Pacific Ocean, respectively, suggesting a strengthening of Walker circulation during the austral summer (Fig. 6d) (Wills et al. 2017). The strengthening of zonal circulation enhances wind convergence over the SAM (Fig. 6d). The change in vertical motion is coordinated by the convergence over the lower troposphere and the divergence over the upper troposphere. The changes in the 200-hPa divergent winds show divergence centered over the eastern Indian Ocean and South America. This ascent is responsible for the increase of ascending motion, which leads to the increase of precipitation over the SH monsoon region.

The enhancement of monsoon circulation could be quantified by the circulation index and the strength of SH subtropical highs (Fig. 7). Following previous studies, the Australian monsoon circulation index is defined as the 850-hPa zonal wind difference between 0° – 15°S , 90° – 130°E and 20° – 30°S , 100° – 140°E ; the SAM circulation index is the 850-hPa zonal wind difference between 5° – 15°S , 70° – 40°W and 22.5° – 30°S , 60° – 40°W ; and the SAF monsoon circulation index is the 700-hPa zonal wind difference between 5° – 15°S , 10° – 30°E and 22.5° – 30°S , 15° – 30°E (Yim et al. 2014; Jin et al. 2020). Figure 7a shows the evolution of the three regional monsoon circulation indices and their average, which is defined as the SH monsoon circulation index. A strengthening of the SH monsoon circulation index indicates an enhancement of monsoon flow convergence, which could result in the increase of monsoon precipitation dynamically and vice versa. In NOAA-20C, the calculated SH monsoon circulation index shows a significant ($p < 0.01$) increase trend during 1901–2014, consistent with the increase of circulation effect.

The strengthening of the SH monsoon circulation is associated with the intensification of the SH subtropical highs. The SH subtropical high index is defined as the 500-hPa geopotential height anomaly over the subtropical high region departure from area-averaged geopotential height over 20° – 40°S , 0° – 360°

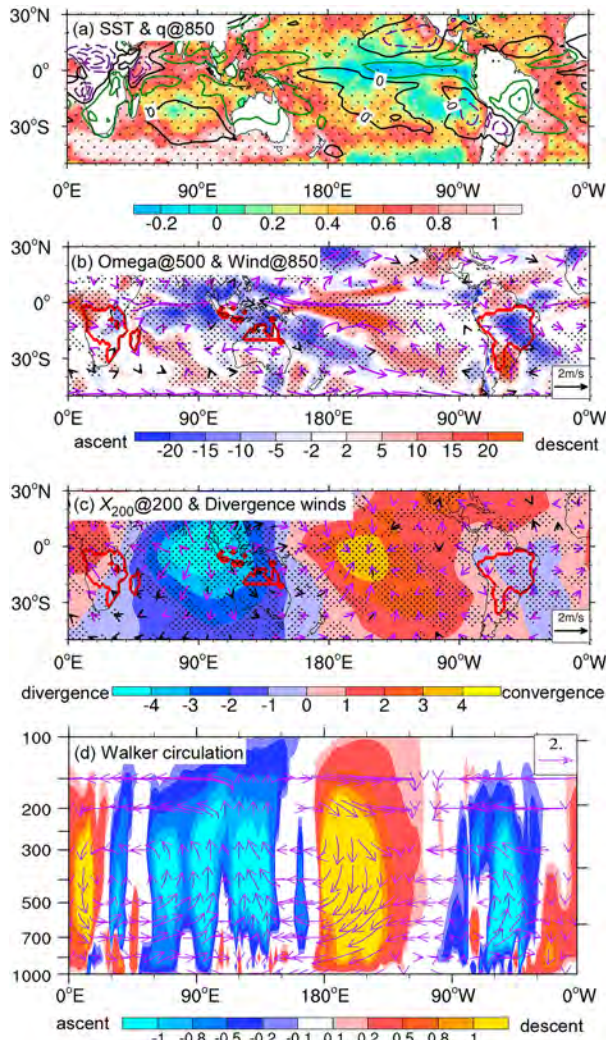


FIG. 6. (a) Trends of SST (shading; K century⁻¹) and 850-hPa specific humidity (contours; g kg⁻¹ century⁻¹). (b) Trends of 500-hPa vertical pressure velocity (shading, 100 × omega; Pa s⁻¹ century⁻¹) and 850-hPa circulation (vectors; m s⁻¹ century⁻¹). (c) Linear trends of velocity potential (shading; 10⁶ m² s⁻¹ century⁻¹) and divergence winds (vectors; m s⁻¹ century⁻¹). (d) Trends of vertical pressure velocity (shading; hPa day⁻¹) and the Walker circulation (vectors) averaged over 20°S–0°. The purple and green lines in (a) indicate the positive and negative trends of 850-hPa specific humidity, respectively, with the zero line plotting in black. Dots represent the trends of precipitation significant at a 90% confidence level. Purple vectors represent the trends of circulation significant at a 90% confidence level.

(He et al. 2015). The South Indian, Pacific, and Atlantic subtropical highs are within the band of 20°–40°S with a longitudinal extension of 50°–110°E, 160°E–80°W, and 40°W–0°, respectively. This geopotential high index has significantly increased from 1901 to 2014 ($p < 0.01$), suggesting the strengthening of the SH subtropical high (Fig. 7b). It increases the moisture redistribution from the tropical ocean to the monsoon region, resulting in the wetting of SH

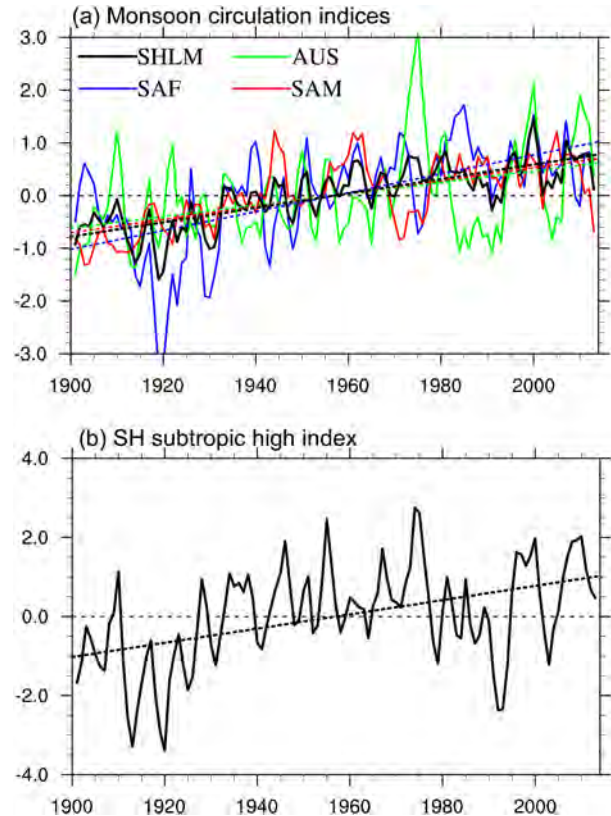


FIG. 7. (a) SH monsoon and three regional monsoon (SAF, AUS, SAM) circulation indices. (b) Change in SH subtropical highs index (gpm). The dashed lines indicate linear trends. SH monsoon circulation index is the average of the three regional monsoon indices.

monsoon. The enhancement of SH subtropical high is partially due to the relative cold SST over the central Pacific, which initiates the descending Rossby wave over its southwest (Fig. 6b). The lower troposphere anticyclonic circulation response enhances the surface wind speed that, in turn, cools the SST over the southeastern Pacific Ocean. Thus, air–sea interaction could further amplify the anticyclonic circulation through ocean upwelling (Seager et al. 2003) and the wind–evaporation–SST feedback (Xie and Philander 1994), leading to the strengthening of the South Pacific subtropical high. Li et al. (2013) suggested that the increase of diabatic heating over the SH continents could strengthen the SH subtropical highs in austral summer. The positive feedback between the SH monsoon and subtropical highs may also contribute to the enhancement of the SH subtropical high (Fig. 7b).

In sum, we found a long-term wetting of SH monsoon, half of which is attributable to the enhancement of monsoon circulation-related moisture convergence, and one-fifth of which is traced back to the increase of atmospheric moisture content. The circulation effect is rooted in the tropical zonal SST gradient. Observation shows an enhancement of the SST gradient between the Indo-Pacific and the eastern Pacific. It

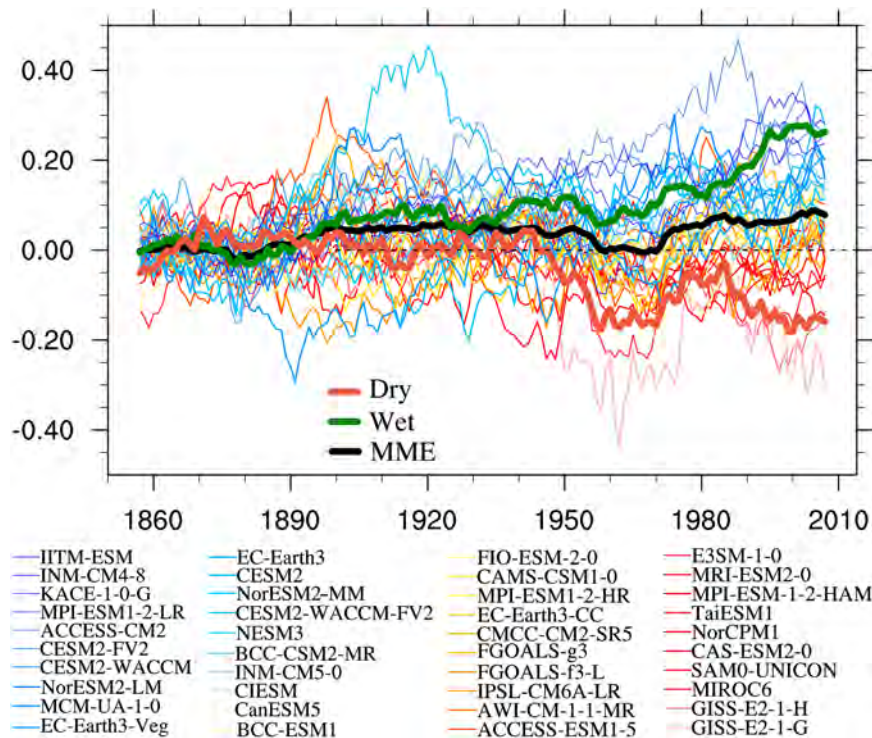


FIG. 8. Evolution of SH monsoon precipitation anomalies in 40 CMIP6 models relative to 1851–80. Thin lines show the 15-yr running mean of SH monsoon precipitation in the individual model. The thick brown and green lines indicate the ensemble mean of four models with the largest dry and wet linear trends during 1851–2014, respectively. The thick black line denotes the multimodel ensemble mean.

increases the sea level pressure gradient across the tropical Pacific, driving the westerly from the Indian Ocean and the easterly from the central Pacific, resulting in the enhanced lower-troposphere moisture convergence. The increases in atmospheric instability promote the ascending motion and upper-troposphere divergence over the Maritime Continent, generating the wettening of the Australian monsoon. The enhanced zonal circulation further increases the lower-troposphere convergence and midlevel ascending motion over South America and eastern South Africa. With the help of strengthened SH subtropical highs, the atmospheric moisture is further transported to the subtropical regions, leading to the increase of SH monsoon precipitation. Thus, the change in tropical SST gradient strengthens the SH monsoons.

c. CMIP6 historical simulations confirm the mechanism

Does this mechanism work in current state-of-the-art climate models? We utilized the historical simulations from 40 CMIP6 models to verify the causality between the wettening of SH monsoon and SST gradient across the tropics. Figure 8 shows the time series of SH monsoon precipitation anomaly in the CMIP6 multimodel mean, the four largest wetting model mean, and the four largest drying model mean for the period of 1851–2014. The multimodel mean has a positive trend of SH monsoon during 1851–2014, with 70% of the models having an increasing trend. The multimodel mean has

an upward trend of $+0.034 \text{ mm day}^{-1} \text{ century}^{-1}$, which is much smaller than the standard deviation ($0.082 \text{ mm day}^{-1} \text{ century}^{-1}$) of the 40 models' linear trends. It degrades the reliability of the wettening of SH monsoon from the multimodel mean. To further explore what controls the wettening or drying of SH monsoon in CMIP6 models, we selected the four models with the largest positive trends as the wet group (IITM-ESM, INM-CM4-8, KACE-1-0-G, MPI-ESM1-2-LR) and the four models with the largest negative trends as the dry group (GISS-E2-1-G, GISS-E2-1-H, MIROC6, SAM0-UNICON). The wet group and dry group have linear trends of $+0.15$ and $-0.12 \text{ mm day}^{-1} \text{ century}^{-1}$, respectively. The trend of the wet group is comparable to the observed one ($+0.14 \text{ mm day}^{-1} \text{ century}^{-1}$) and smaller than that in the reanalysis datasets ($+0.73 \text{ mm day}^{-1} \text{ century}^{-1}$ in NOAA-20C and $+0.62 \text{ mm day}^{-1} \text{ century}^{-1}$ in ERA-20C).

Why can some models successfully capture the wettening of SH monsoon, but some models fail? Figure 9 compares the difference in linear trends between the wet and dry groups. This is used to confirm whether the physical processes obtained from the observation work or not. All the observed phenomena are well depicted in figures of the difference between wet and dry groups. Compared to the dry group, the surface temperature pattern in the wet group shows a larger warming over the Maritime Continent and equatorial western Pacific and less warming over the eastern Pacific Ocean.

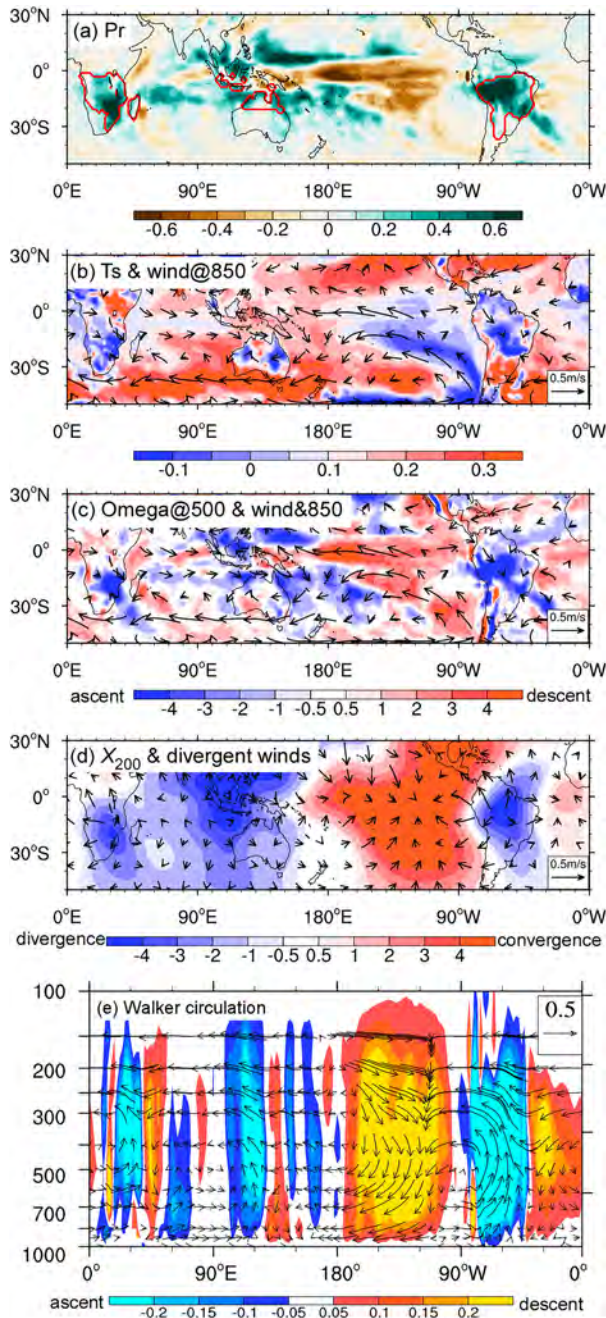


FIG. 9. Difference in linear trends between the wet and dry models during 1851–2014, for (a) for precipitation ($\text{mm day}^{-1} \text{ century}^{-1}$), (b) surface temperature (shading; K century^{-1}) and 850-hPa circulation ($\text{m s}^{-1} \text{ century}^{-1}$), (c) 500-hPa vertical pressure velocity (shading; $100 \times \text{omega}$; $\text{Pa s}^{-1} \text{ century}^{-1}$) and 850-hPa circulation ($\text{m s}^{-1} \text{ century}^{-1}$), (d) velocity potential (shading; $10^5 \text{ m}^2 \text{ s}^{-1} \text{ century}^{-1}$) and divergence winds ($\text{m s}^{-1} \text{ century}^{-1}$) at 200 hPa, and (e) vertical pressure velocity (shading; hPa day^{-1}) and the difference in Walker circulation (vectors) averaged over 20°S – 0° .

Correspondingly, the lower-troposphere circulation response to the temperature pattern is characterized by the westerly over the equatorial Indian Ocean and easterly over the equatorial Pacific Ocean (Fig. 9b). The precipitation pattern shows the wetting over the majority of the Indo-Pacific region, as well as the SH monsoon regions, and drying over the equatorial central Pacific (Fig. 9a). It suggests that the models that simulate the SST contrast well between the Indo-Pacific and eastern Pacific can reproduce the SH monsoon wetting trend over the historical period, while models that fail to simulate the SST gradient do not reproduce the observed SH monsoon precipitation change.

The increase in SH monsoon precipitation in the wet group is largely driven by enhanced monsoon circulation, midlevel ascending motion, and upper-troposphere divergence flow. As shown in Fig. 9c, low-latitude westerly and extratropical easterlies are both enhanced over the AUS, and an enhancement of cross-equatorial flow and monsoon circulation is evident over the SAM. Therefore, the monsoon circulation index would increase, meaning the strengthening of monsoonal moisture convergence. The change in midlevel velocity shows the enhanced ascending motion over the Indo-Pacific, SAM, and eastern SAF, while descending motion over the eastern Pacific and tropical Atlantic. This vertical motion response is consistent with the upper-level divergent winds. It shows divergence centers over the SAF, AUS, and SAM regions and convergence over the eastern Pacific and tropical Atlantic, resulting in the enhancement of midtroposphere ascending motion and convection (Figs. 9c–e). A similar analysis is also performed for 1901–2014; it yields similar results as shown in Figs. 8 and 9 (figure not shown). Therefore, the response of monsoon circulation benefits the wetting of SH monsoon in the models with larger surface temperature contrast between the Indo-Pacific and eastern Pacific Oceans. This is consistent with the processes identified in the NOAA-20C.

The above analysis demonstrates the important role of zonal SST gradient for SH monsoons. However, what drives the observed and simulated zonal SST gradient changes during 1901–2014 remains an open question. The zonal SST gradient (Z_SST) is quantified by the SST difference between the Indo-Pacific region (20°S – 10°N , 90° – 150°E) and eastern Pacific region (20°S – 10°N , 150° – 80°W). Figure 10a shows that the Z_SST index significantly increased during 1901–2014 in the Hadley SST dataset. The SST gradient has a periodicity of 3–7 years (figure not shown), indicating the critical role of El Niño–Southern Oscillation. There is no clear multidecadal oscillation of the zonal SST gradient, suggesting the observed zonal SST gradient may be a part of centennial or longer time scale variation from Earth system internal modes or external forcing (Seager et al. 2019; Coats and Karnauskas 2017). The ensemble mean of the 40 CMIP6 historical simulations suggests a small change of zonal SST gradient with a larger inter-model spread ($-0.021 \pm 0.11 \text{ K century}^{-1}$) during 1851–2014. If the observed zonal SST gradient change is caused by anthropogenic forcing, one would expect a high consensus of the simulated SST gradient change during the historical period. Seager et al. (2019) demonstrated that the observed

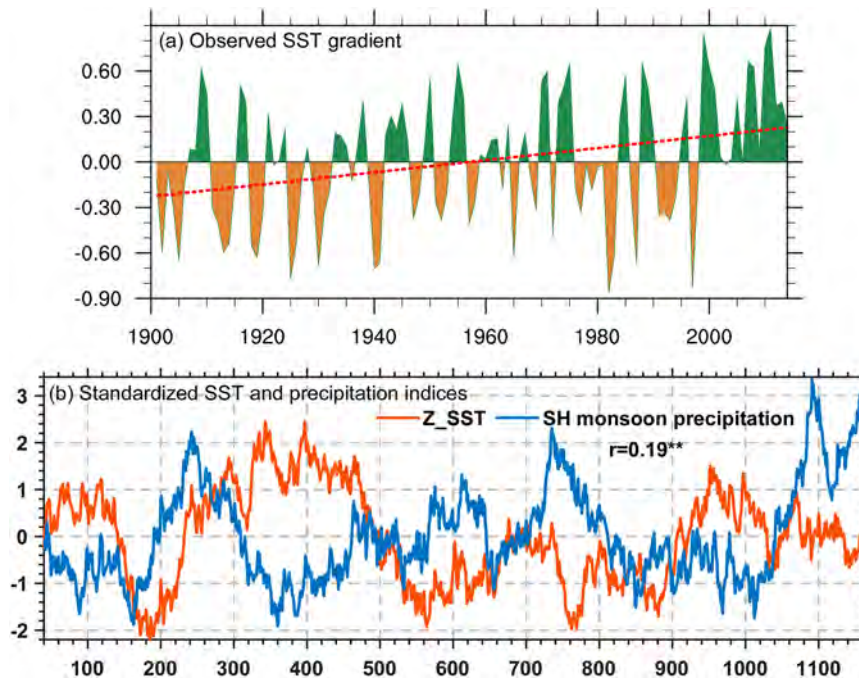


FIG. 10. (a) Observed zonal SST gradient (Indo-Pacific region minus eastern Pacific region) index relative to the average of 1901–2014. (b) Standardized zonal SST gradient index and SH monsoon precipitation index after the 79-yr running mean in CESM preindustrial simulation. Two asterisks (**) indicate significance at a 99% confidence level.

enhancement of zonal SST gradient comes from the increase of greenhouse gases using a simplified ocean–atmosphere coupled model. They pointed out that the failure in simulating this zonal SST gradient change is due to the cold tongue SST bias in climate models. The centennial Z_SST trend is possibly generated by the Earth system’s internal dynamics (Coats and Karnauskas 2017). Figure 10b shows the evolution of Z_SST index from the preindustrial simulation of the CESM2 model. With the permanent fixed external forcing, the CESM2 model can simulate apparent zonal SST gradient variation on the centennial time scale. This SST gradient change is coherent with the SH monsoon precipitation change, suggesting that the Earth system’s internal mode may play a role in the observed wetting of SH monsoons (Fig. 10b).

d. Critical role of monsoon ascending to Hadley cell movement during the historical period

The causality between the swing of ITCZ/Hadley circulation and the strength of SH monsoon is still in debate. We assess this issue by examining the contribution of anomalous meridional divergent circulation over the monsoon and non-monsoon regions (Trenberth et al. 2000). Figure 11 shows the regional meridional divergent circulation averaged over the SH monsoon band and non-monsoon band, as well as the zonal mean Hadley cell. The monsoon band is the sum of three monsoon regions over 10° – 50° E, 110° – 150° E, and 80° – 40° W, respectively. The monsoon band only accounts for 1/3 of global longitude, and the other 2/3 of the global longitude is the non-monsoon band. The shading of Figs. 11a and 11d show the zonal mean

climatological vertical pressure velocity as an indication of Hadley cell. In both NOAA-20C and CMIP6 simulations, the ascending motion occupies the meridional band of 20° S– 10° N, and the descent resides on both sides of this ascending motion. The linear trend of zonal mean meridional circulation shows the enhancement of vertical motion in 10° – 25° S, which covers the meridional extent of SH monsoons, suggesting the southward movement and strengthening of the climatological Hadley cell. This is consistent with the increase in SH monsoon and southward movement of the ITCZ. The difference in wet and dry models from CMIP6 historical simulations confirms the observed changes in the Hadley cell (Fig. 11d).

What is the source of this southward movement and strengthening of Hadley cell during 1901–2014? The regional meridional circulation over the monsoon and non-monsoon bands demonstrated distinct changes (Figs. 11b,c). The southward movement and strengthening of regional meridional circulation can only be observed over the monsoon band (Fig. 11b). In contrast, the non-monsoon band is occupied by the anomalous descending motion, especially over 0° – 20° S (Fig. 11c). Without the contribution from the monsoon band, the zonal Hadley circulation would be weakened, instead of strengthening in the observation (Fig. 11a). Therefore, the ascending motion over the monsoon band is vital for enhancing the zonal mean Hadley circulation during austral summer (Trenberth et al. 2000). This phenomenon is clearly shown in both reanalysis and model simulations, suggesting that it may be a robust process. From this perspective, the change in zonal mean Hadley cell is

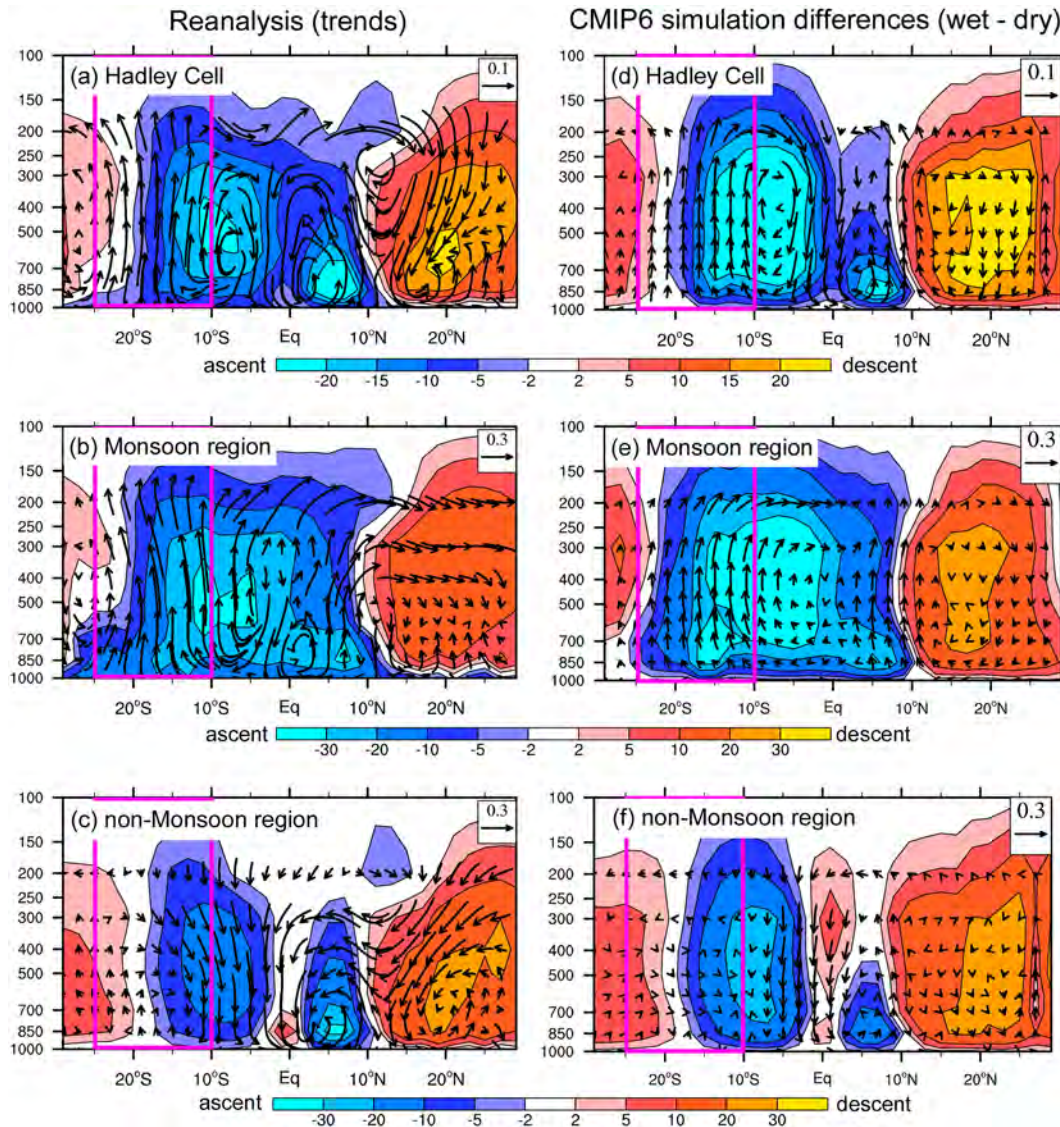


FIG. 11. Austral summer (DJFM) climatology vertical pressure velocity (shading; hPa day^{-1}) and linear trends of meridional divergence circulation (vectors) from (left) NOAA-20C reanalysis during 1901–2014 and (right) difference in wet and dry CMIP6 models during 1851–2014. (a) Zonal averaged Hadley circulation. (b) As in (a), but for the monsoon region (10° – 50°E , 110° – 150°E , and 80° – 40°W). (c) As in (a), but for the non-monsoon region. (d)–(f) As in (a)–(c), but for the difference between wet and dry models. Vector is the composite of 100 times vertical velocity change ($\text{Pa s}^{-1} \text{ century}^{-1}$) with meridional wind trend ($\text{m s}^{-1} \text{ century}^{-1}$). The purple boxes indicate the meridional extent of the SH monsoon region.

dominated by the regional meridional circulation over the monsoon region. The usage of changes in the Hadley cell to explain the monsoon precipitation should be taken with caution (Trenberth et al. 2000; Wang et al. 2014, 2017; Wang et al. 2021).

4. Conclusions

Paleo-proxy data and simulations suggest that the changes in SH monsoons are not always coherent with the NH counterpart (Wang et al. 2006; Cheng et al. 2012; Liu et al. 2009; Cao et al. 2022). The consensus of future projected changes in

NH monsoons is relatively high, while the changes in SH monsoons are insignificant and highly uncertain (Wang et al. 2020; Chen et al. 2020; D'Agostino et al. 2019, 2020). Constraining the future projection of the SH monsoon requires a deep understanding of the physical processes and mechanisms during the instrumental period. Unlike the decline in NH monsoon in the past century (1901–2014) (Cao et al. 2022), we revealed a significant increase in SH monsoon precipitation in observations during 1901–2014. Both twentieth-century reanalysis data from NOAA and ECMWF confirmed the significant long-term wetting of SH monsoon from 1901

to 2014. This wettening is more evident over the Australian and South American monsoon regions in both observation and reanalysis. A moisture budget analysis is used to disentangle the processes responsible for it. The results from NOAA-20C suggest that the enhancement of monsoon circulation explains half of the wettening in SH monsoon, while only one-fifth is attributable to atmospheric moistening. The warming of the global surface enhances the lower-troposphere moisture, which explains the increase of the moisture effect. The circulation effect is attributed to the enhanced lower-troposphere monsoonal convergence. The circulation effect also largely explains the interannual to decadal-scale change of the SH monsoon.

The change in SH monsoon circulation is related to the east–west SST gradient across the tropics. This is distinct from the vital role of the north–south thermal contrast on NH monsoon circulation (e.g., Liu et al. 2012). During the austral summer, the trend in SST is characterized by greater warming over the Indo-Pacific and less warming/cooling over the eastern Pacific (Seager et al. 2019). This surface temperature gradient drives the lower-troposphere circulation change, resulting in the westerly anomaly over the Indo-Pacific region and easterly anomaly over the equatorial Pacific Ocean. It enhances the climatological Walker circulation, showing anomalous ascending motion over the Maritime Continent and descending motion over the central Pacific. The change in tropical zonal circulation further enhances the ascending motion over South America. Therefore, the SH monsoon region is dominated by anomalous moisture convergence and convection, leading to an increase in SH monsoon precipitation. This physical process is well depicted in the wet group model of CMIP6 historical simulations, which shows the wettening of SH monsoon. The models that failed to simulate this zonal SST gradient suggest the drying of SH monsoon. Further analysis found that the wet models simulated greater warming over the Indo-Pacific and less warming over the eastern Pacific, westerly anomalies and easterly anomalies straddling the Maritime Continent, and an increase in moisture convergence over SAF, AUS, and SAM. Therefore, a successful simulation of this zonal SST gradient is fundamental to reproducing the observed wettening of SH monsoon during the historical period. This physical process could be used to constrain the future projected SH monsoon (Cao et al. 2020; Chen et al. 2020). As the globe warms, the thermodynamic effect increases the monsoon precipitation, while the projected El Niño-like warming (Collins et al. 2011) results in a weakened circulation effect. The canceling of the thermodynamic and circulation effect may yield an insignificant change in SH monsoon precipitation. Thus, a better simulation of the tropical SST gradient change may lead to an accurate projection of future SH monsoons.

Another finding is that the SH monsoonal convergence is vital for the observed change in the austral summer Hadley cell (Fig. 11). This is different from many prior studies, which often use the zonal mean Hadley circulation to explain the SH monsoon changes (e.g., Wang et al. 2006; Cheng et al. 2012). We found that the changes in meridional circulation over the monsoon region dominate the enhancement and poleward movement of the austral summer Hadley cell in the NOAA-20C reanalysis and CMIP6 simulations. The non-

monsoonal meridional circulation tends to mitigate this change. In this perspective, the strengthening of monsoon circulation may cause the movement of Hadley cell and ITCZ (Trenberth et al. 2000).

Acknowledgments. Jian Cao acknowledges the support from the Natural Science Foundation of China of Jiangsu Province (BK20220108) and the Natural Science Foundation of China (42005017, 42375034). Xiaowei Zhu acknowledges the support from Key Research and Development program of Ningxia (2022BEG03058) and the Natural Science Foundation of China of Ningxia (2022AAC03673). Hao Wang acknowledges the support from the Postgraduate Research and Practice Innovation Program of Jiangsu Province (KYCX23_1328). We acknowledge the computer resources at the NUIST High Performance Computer Center. The authors confirm that there are no known conflicts of interest associated with this article.

Data availability statement. The CMIP6 model data are available from <https://esgf-node.llnl.gov/projects/cmip6/>. We acknowledge the World Climate Research Programme's Working Group on Coupled Modelling, which is responsible for CMIP.

REFERENCES

- Alexander, L. V., M. Bador, R. Roca, S. Contractor, M. G. Donat, and P. L. Nguyen, 2020: Intercomparison of annual precipitation indices and extremes over global land areas from in situ, space-based and reanalysis products. *Environ. Res. Lett.*, **15**, 055002, <https://doi.org/10.1088/1748-9326/ab79e2>.
- An, Z., and Coauthors, 2015: Global monsoon dynamics and climate change. *Annu. Rev. Earth Planet. Sci.*, **43**, 29–77, <https://doi.org/10.1146/annurev-earth-060313-054623>.
- Biasutti, M., and Coauthors, 2018: Global energetics and local physics as drivers of past, present and future monsoons. *Nat. Geosci.*, **11**, 392–400, <https://doi.org/10.1038/s41561-018-0137-1>.
- Bischoff, T., and T. Schneider, 2014: Energetic constraints on the position of the intertropical convergence zone. *J. Climate*, **27**, 4937–4951, <https://doi.org/10.1175/JCLI-D-13-00650.1>.
- Bollasina, M. A., Y. Ming, and V. Ramaswamy, 2011: Anthropogenic aerosols and the weakening of the South Asian summer monsoon. *Science*, **334**, 502–505, <https://doi.org/10.1126/science.1204994>.
- Boos, W. R., and R. L. Korty, 2016: Regional energy budget control of the intertropical convergence zone and application to mid-Holocene rainfall. *Nat. Geosci.*, **9**, 892–897, <https://doi.org/10.1038/ngeo2833>.
- Bordoni, S., and T. Schneider, 2008: Monsoons as eddy-mediated regime transitions of the tropical overturning circulation. *Nat. Geosci.*, **1**, 515–519, <https://doi.org/10.1038/ngeo248>.
- Broccoli, A. J., K. A. Dahl, and R. J. Stouffer, 2006: Response of the ITCZ to Northern Hemisphere cooling. *Geophys. Res. Lett.*, **33**, L01702, <https://doi.org/10.1029/2005GL024546>.
- Brown, J. R., A. F. Moise, R. Colman, and H. Zhang, 2016: Will a warmer world mean a wetter or drier Australian monsoon? *J. Climate*, **29**, 4577–4596, <https://doi.org/10.1175/JCLI-D-15-0695.1>.
- Cao, J., and H.-K. Zhao, 2020: Distinct response of Northern Hemisphere land monsoon precipitation to transient and

- stabilized warming scenarios. *Adv. Climate Change Res.*, **11**, 161–171, <https://doi.org/10.1016/j.accre.2020.09.007>.
- , B. Wang, and J. Liu, 2019a: Attribution of the last glacial maximum climate formation. *Climate Dyn.*, **53**, 1661–1679, <https://doi.org/10.1007/s00382-019-04711-6>.
- , —, and L. Ma, 2019b: Attribution of global monsoon response to the last glacial maximum forcings. *J. Climate*, **32**, 6589–6605, <https://doi.org/10.1175/JCLI-D-18-0871.1>.
- , —, B. Wang, H. Zhao, C. Wang, and Y. Han, 2020: Sources of the intermodel spread in projected global monsoon hydrological sensitivity. *Geophys. Res. Lett.*, **47**, e2020GL089560, <https://doi.org/10.1029/2020GL089560>.
- , and Coauthors, 2021: NUIST ESM v3 data submission to CMIP6. *Adv. Atmos. Sci.*, **38**, 268–284, <https://doi.org/10.1007/s00376-020-0173-9>.
- , H. Wang, B. Wang, H. Zhao, C. Wang, and X. Zhu, 2022: Higher sensitivity of Northern Hemisphere monsoon to anthropogenic aerosol than greenhouse gases. *Geophys. Res. Lett.*, **49**, e2022GL100270, <https://doi.org/10.1029/2022GL100270>.
- Chadwick, R., I. Boutle, and G. Martin, 2013: Spatial patterns of precipitation change in CMIP5: Why the rich do not get richer in the tropics. *J. Climate*, **26**, 3803–3822, <https://doi.org/10.1175/JCLI-D-12-00543.1>.
- Charney, J. G., 1969: A further note on large-scale motions in the tropics. *J. Atmos. Sci.*, **26**, 182–185, [https://doi.org/10.1175/1520-0469\(1969\)026<0182:AFNOLS>2.0.CO;2](https://doi.org/10.1175/1520-0469(1969)026<0182:AFNOLS>2.0.CO;2).
- Chen, Z., T. Zhou, L. Zhang, X. Chen, W. Zhang, and J. Jiang, 2020: Global land monsoon precipitation changes in CMIP6 projections. *Geophys. Res. Lett.*, **47**, e2019GL086902, <https://doi.org/10.1029/2019GL086902>.
- Cheng, H., A. Sinha, X. Wang, F. W. Cruz, and R. L. Edwards, 2012: The global paleomonsoon as seen through speleothem records from Asia and the Americas. *Climate Dyn.*, **39**, 1045–1062, <https://doi.org/10.1007/s00382-012-1363-7>.
- Chou, C., J. D. Neelin, C.-A. Chen, and J.-Y. Tu, 2009: Evaluating the “rich-get-richer” mechanism in tropical precipitation change under global warming. *J. Climate*, **22**, 1982–2005, <https://doi.org/10.1175/2008JCLI2471.1>.
- Coats, S., and K. B. Karnauskas, 2017: Are simulated and observed twentieth century tropical Pacific sea surface temperature trends significant relative to internal variability? *Geophys. Res. Lett.*, **44**, 9928–9937, <https://doi.org/10.1002/2017GL074622>.
- Collins, J., and Coauthors, 2011: Interhemispheric symmetry of the tropical African rainbelt over the past 23,000 years. *Nat. Geosci.*, **4**, 42–45, <https://doi.org/10.1038/ngeo1039>.
- Compo, G. P., and Coauthors, 2011: The Twentieth Century Reanalysis Project. *Quart. J. Roy. Meteor. Soc.*, **137** (654), 1–28, <https://doi.org/10.1002/qj.776>.
- D’Agostino, R., J. Bader, S. Bordoni, D. Ferreira, and J. Jungclauss, 2019: Northern Hemisphere monsoon response to mid-Holocene orbital forcing and greenhouse gas-induced global warming. *Geophys. Res. Lett.*, **46**, 1591–1601, <https://doi.org/10.1029/2018GL081589>.
- , J. R. Brown, A. Moise, H. Nguyen, P. L. S. Dias, and J. Jungclauss, 2020: Contrasting Southern Hemisphere monsoon response: Mid-Holocene orbital forcing versus future greenhouse gas-induced global warming. *J. Climate*, **33**, 9595–9613, <https://doi.org/10.1175/JCLI-D-19-0672.1>.
- Donohoe, A., J. Marshall, D. Ferreira, and D. Mcgee, 2013: The relationship between ITCZ location and cross-equatorial atmospheric heat transport: From the seasonal cycle to the last glacial maximum. *J. Climate*, **26**, 3597–3618, <https://doi.org/10.1175/JCLI-D-12-00467.1>.
- Endo, H., and A. Kitoh, 2014: Thermodynamic and dynamic effects on regional monsoon rainfall changes in a warmer climate. *Geophys. Res. Lett.*, **41**, 1704–1711, <https://doi.org/10.1002/2013GL059158>.
- Eyring, V., S. Bony, G. A. Meehl, C. A. Senior, B. Stevens, R. J. Stouffer, and K. E. Taylor, 2016: Overview of the Coupled Model Intercomparison Project Phase 6 (CMIP6) experimental design and organization. *Geosci. Model Dev.*, **9**, 1937–1958, <https://doi.org/10.5194/gmd-9-1937-2016>.
- Frierson, D. M. W., and Coauthors, 2013: Contribution of ocean overturning circulation to tropical rainfall peak in the Northern Hemisphere. *Nat. Geosci.*, **6**, 940–944, <https://doi.org/10.1038/ngeo1987>.
- Gadgil, S., 2018: The monsoon system: Land–sea breeze or the ITCZ? *J. Earth Syst. Sci.*, **127**, 1, <https://doi.org/10.1007/s12040-017-0916-x>.
- Geen, R., S. Bordoni, D. S. Battisti, and K. Hui, 2020: Monsoons, ITCZs, and the concept of the global monsoon. *Rev. Geophys.*, **58**, e2020RG000700, <https://doi.org/10.1029/2020RG000700>.
- Ha, K.-J., B.-H. Kim, E.-S. Chung, J. C. L. Chan, and C.-P. Chang, 2020: Major factors of global and regional monsoon rainfall changes: Natural versus anthropogenic forcing. *Environ. Res. Lett.*, **15**, 034055, <https://doi.org/10.1088/1748-9326/ab7767>.
- Harris, I., P. D. Jones, T. J. Osborn, and D. H. Lister, 2014: Updated high-resolution grids of monthly climatic observations—The CRU TS3.10 dataset. *Int. J. Climatol.*, **34**, 623–642, <https://doi.org/10.1002/joc.3711>.
- He, C., T. Zhou, A. Lin, B. Wu, D. Gu, C. Li, and B. Zheng, 2015: Enhanced or weakened western North Pacific subtropical high under global warming? *Sci. Rep.*, **5**, 16771, <https://doi.org/10.1038/srep16771>.
- Held, I. M., and B. J. Soden, 2006: Robust responses of the hydrological cycle to global warming. *J. Climate*, **19**, 5686–5699, <https://doi.org/10.1175/JCLI3990.1>.
- Hsu, P.-C., T. Li, J.-J. Luo, H. Murakami, A. Kitoh, and M. Zhao, 2012: Increase of global monsoon area and precipitation under global warming: A robust signal? *Geophys. Res. Lett.*, **39**, L06701, <https://doi.org/10.1029/2012GL051037>.
- , —, H. Murakami, and A. Kitoh, 2013: Future change of the global monsoon revealed from 19 CMIP5 models. *J. Geophys. Res. Atmos.*, **118**, 1247–1260, <https://doi.org/10.1002/jgrd.50145>.
- Huang, X., T. Zhou, W. Zhang, J. Jiang, P. Li, and Y. Zhao, 2019: Northern Hemisphere land monsoon precipitation changes in the twentieth century revealed by multiple reanalysis sets. *Climate Dyn.*, **53**, 7131–7149, <https://doi.org/10.1007/s00382-019-04982-z>.
- Jiang, D., Z. Tian, and X. Lang, 2015: Mid-Holocene global monsoon area and precipitation from PMIP simulations. *Climate Dyn.*, **44**, 2493–2512, <https://doi.org/10.1007/s00382-014-2175-8>.
- Jin, C., B. Wang, and J. Liu, 2020: Future changes and controlling factors of the eight regional monsoons projected by CMIP6 models. *J. Climate*, **33**, 9307–9326, <https://doi.org/10.1175/JCLI-D-20-0236.1>.
- Kalnay, E., and Coauthors, 1996: The NCEP/NCAR 40-Year Reanalysis Project. *Bull. Amer. Meteor. Soc.*, **77**, 437–472, [https://doi.org/10.1175/1520-0477\(1996\)077<0437:TNYRP>2.0.CO;2](https://doi.org/10.1175/1520-0477(1996)077<0437:TNYRP>2.0.CO;2).
- Kendall, M. G., 1955: Further contributions to the theory of paired comparisons. *Biometrics*, **11**, 43–62, <https://doi.org/10.2307/3001479>.
- Kobayashi, S., and Coauthors, 2015: The JRA-55 reanalysis: General specifications and basic characteristics. *J. Meteor. Soc. Japan*, **93**, 5–48, <https://doi.org/10.2151/jmsj.2015-001>.

- Lee, J.-Y., and B. Wang, 2014: Future change of global monsoon in the CMIP5. *Climate Dyn.*, **42**, 101–119, <https://doi.org/10.1007/s00382-012-1564-0>.
- Li, Q., J. Cao, and H. Zhao, 2022: On the anti-phase relationship of the Northern and Southern Hemisphere monsoon precipitation over the past 20000 years. *Quat. Sci.*, **42**, 325–337, <https://doi.org/10.11928/j.issn.1001-7410.2022.02.01>.
- Li, W., and Coauthors, 2013: Intensification of the Southern Hemisphere summertime subtropical anticyclones in a warming climate. *Geophys. Res. Lett.*, **40**, 5959–5964, <https://doi.org/10.1002/2013GL058124>.
- Lin, R., T. Zhou, and Y. Qian, 2014: Evaluation of global monsoon precipitation changes based on five reanalysis datasets. *J. Climate*, **27**, 1271–1289, <https://doi.org/10.1175/JCLI-D-13-00215.1>.
- Liu, J., B. Wang, Q. Ding, X. Kuang, W. Soon, and E. Zorita, 2009: Centennial variations of the global monsoon precipitation in the last millennium: Results from ECHO-G model. *J. Climate*, **22**, 2356–2371, <https://doi.org/10.1175/2008JCLI2353.1>.
- , —, S.-Y. Yim, J.-Y. Lee, J.-G. Jhun, and K.-J. Ha, 2012: What drives the global summer monsoon over the past millennium? *Climate Dyn.*, **39**, 1063–1072, <https://doi.org/10.1007/s00382-012-1360-x>.
- Marshall, G. J., 2003: Trends in the Southern Annular Mode from observations and reanalyses. *J. Climate*, **16**, 4134–4143, [https://doi.org/10.1175/1520-0442\(2003\)016<4134:TITSAM>2.0.CO;2](https://doi.org/10.1175/1520-0442(2003)016<4134:TITSAM>2.0.CO;2).
- Monerie, P., L. J. Wilcox, and A. G. Turner, 2022: Effects of anthropogenic aerosol and greenhouse gas emissions on Northern Hemisphere monsoon precipitation: Mechanisms and uncertainty. *J. Climate*, **35**, 2305–2326, <https://doi.org/10.1175/JCLI-D-21-0412.1>.
- Poli, P., and Coauthors, 2016: ERA-20C: An atmospheric reanalysis of the twentieth century. *J. Climate*, **29**, 4083–4097, <https://doi.org/10.1175/JCLI-D-15-0556.1>.
- Polson, D., M. Bollasina, G. C. Hegerl, and L. J. Wilcox, 2014: Decreased monsoon precipitation in the Northern Hemisphere due to anthropogenic aerosols. *Geophys. Res. Lett.*, **41**, 6023–6029, <https://doi.org/10.1002/2014GL060811>.
- Rayner, N. A., D. E. Parker, E. B. Horton, C. K. Folland, L. V. Alexander, D. P. Rowell, E. C. Kent, and A. Kaplan, 2003: Global analyses of sea surface temperature, sea ice, and night marine air temperature since the late nineteenth century. *J. Geophys. Res.*, **108**, 4407, <https://doi.org/10.1029/2002JD002670>.
- Schneider, T., T. Bischoff, and G. H. Haug, 2014: Migrations and dynamics of the intertropical convergence zone. *Nature*, **513**, 45–53, <https://doi.org/10.1038/nature13636>.
- Schneider, U., A. Becker, P. Finger, A. Meyer-Christoffer, M. Ziese, and B. Rudolf, 2014: GPCC's new land surface precipitation climatology based on quality-controlled in situ data and its role in quantifying the global water cycle. *Theor. Appl. Climatol.*, **115**, 15–40, <https://doi.org/10.1007/s00704-013-0860-x>.
- Scussolini, P., and Coauthors, 2019: Agreement between reconstructed and modeled boreal precipitation of the last interglacial. *Sci. Adv.*, **5**, eaax7047, <https://doi.org/10.1126/sciadv.aax7047>.
- Seager, R., R. Murthugudde, N. Naik, A. Clement, N. Gordon, and J. Miller, 2003: Air–sea interaction and the seasonal cycle of the subtropical anticyclones. *J. Climate*, **16**, 1948–1966, [https://doi.org/10.1175/1520-0442\(2003\)016<1948:AIATSC>2.0.CO;2](https://doi.org/10.1175/1520-0442(2003)016<1948:AIATSC>2.0.CO;2).
- , N. Naik, and G. A. Vecchi, 2010: Thermodynamic and dynamic mechanisms for large-scale changes in the hydrological cycle in response to global warming. *J. Climate*, **23**, 4651–4668, <https://doi.org/10.1175/2010JCLI3655.1>.
- , M. Cane, N. Henderson, D.-E. Lee, R. Abernathy, and H. Zhang, 2019: Strengthening tropical Pacific zonal sea surface temperature gradient consistent with rising greenhouse gases. *Nat. Climate Change*, **9**, 517–522, <https://doi.org/10.1038/s41558-019-0505-x>.
- Trenberth, K. E., D. P. Stepaniak, and J. M. Caron, 2000: The global monsoon as seen through the divergent atmospheric circulation. *J. Climate*, **13**, 3969–3993, [https://doi.org/10.1175/1520-0442\(2000\)013<3969:TGMASST>2.0.CO;2](https://doi.org/10.1175/1520-0442(2000)013<3969:TGMASST>2.0.CO;2).
- Wang, B., and Q. Ding, 2006: Changes in global monsoon precipitation over the past 56 years. *Geophys. Res. Lett.*, **33**, L06711, <https://doi.org/10.1029/2005GL025347>.
- , J. Liu, H.-J. Kim, P. J. Webster, and S.-Y. Yim, 2012: Recent change of the global monsoon precipitation (1979–2008). *Climate Dyn.*, **39**, 1123–1135, <https://doi.org/10.1007/s00382-011-1266-z>.
- , and Coauthors, 2018: Toward predicting changes in the land monsoon rainfall a decade in advance. *J. Climate*, **31**, 2699–2714, <https://doi.org/10.1175/JCLI-D-17-0521.1>.
- , C. Jin, and J. Liu, 2020: Understanding future change of global monsoons projected by CMIP6 models. *J. Climate*, **33**, 6471–6489, <https://doi.org/10.1175/JCLI-D-19-0993.1>.
- , and Coauthors, 2021: Monsoons climate change assessment. *Bull. Amer. Meteor. Soc.*, **102**, E1–E19, <https://doi.org/10.1175/BAMS-D-19-0335.1>.
- Wang, P. X., B. Wang, H. Cheng, J. Fasullo, Z. T. Guo, T. Kiefer, and Z. Y. Liu, 2014: The global monsoon across timescales: Coherent variability of regional monsoons. *Climate Past*, **10**, 2007–2052, <https://doi.org/10.5194/cp-10-2007-2014>.
- , —, —, —, Z. Guo, T. Kiefer, and Z. Liu, 2017: The global monsoon across time scales: Mechanisms and outstanding issues. *Earth-Sci. Rev.*, **174**, 84–121, <https://doi.org/10.1016/j.earscirev.2017.07.006>.
- Wang, X., A. S. Auler, R. L. Edwards, H. Cheng, E. Ito, and M. Solheid, 2006: Interhemispheric anti-phasing of rainfall during the last glacial period. *Quat. Sci. Rev.*, **25**, 3391–3403, <https://doi.org/10.1016/j.quascirev.2006.02.009>.
- Willmott, C. J., and K. Matsuura, 2001: Terrestrial air temperature and precipitation: Monthly and annual time series (1950–1999), version 1.02. Center for Climatic Research, Department of Geography, University of Delaware, accessed 10 September 2022, http://climate.geog.udel.edu/~climate/html_pages/README.ghcn_ts2.html.
- Wills, R. C., X. J. Levine, and T. Schneider, 2017: Local energetic constraints on Walker circulation strength. *J. Atmos. Sci.*, **74**, 1907–1922, <https://doi.org/10.1175/JAS-D-16-0219.1>.
- Xiang, B., M. Zhao, Y. Ming, W. Yu, and S. M. Kang, 2018: Contrasting impacts of radiative forcing in the Southern Ocean versus southern tropics on ITCZ position and energy transport in one GFDL climate model. *J. Climate*, **31**, 5609–5628, <https://doi.org/10.1175/JCLI-D-17-0566.1>.
- Xie, S.-P., and S. G. H. Philander, 1994: A coupled ocean–atmosphere model of relevance to the ITCZ in the eastern Pacific. *Tellus*, **46A**, 340–350, <https://doi.org/10.1034/j.1600-0870.1994.t01-1-00001.x>.
- Yan, M., B. Wang, and J. Liu, 2016: Global monsoon change during the Last Glacial Maximum: A multi-model study. *Climate Dyn.*, **47**, 359–374, <https://doi.org/10.1007/s00382-015-2841-5>.

- Yim, S.-Y., B. Wang, J. Liu, and Z. Wu, 2014: A comparison of regional monsoon variability using monsoon indices. *Climate Dyn.*, **43**, 1423–1437, <https://doi.org/10.1007/s00382-013-1956-9>.
- Zhang, L., and T. Zhou, 2011: An assessment of monsoon precipitation changes during 1901–2001. *Climate Dyn.*, **37**, 279–296, <https://doi.org/10.1007/s00382-011-0993-5>.
- Zhang, Y., Y. Guo, W. Dong, and C. Li, 2018: What drives the decadal variation of global land monsoon precipitation over the past 50 years? *Int. J. Climatol.*, **38**, 4818–4829, <https://doi.org/10.1002/joc.5699>.
- Zhou, T., R. Yu, H. Li, and B. Wang, 2008: Ocean forcing to changes in global monsoon precipitation over the recent half-century. *J. Climate*, **21**, 3833–3852, <https://doi.org/10.1175/2008JCLI2067.1>.
- , W. Zhang, L. Zhang, X. Zhang, Y. Qian, D. Peng, S. Ma, and B. Dong, 2020a: The dynamic and thermodynamic processes dominating the reduction of global land monsoon precipitation driven by anthropogenic aerosols emission. *Sci. China Earth Sci.*, **63**, 919–933, <https://doi.org/10.1007/s11430-019-9613-9>.
- , J. Lu, W. Zhang, and Z. Chen, 2020b: The sources of uncertainty in the projection of global land monsoon precipitation. *Geophys. Res. Lett.*, **47**, e2020GL088415, <https://doi.org/10.1029/2020GL088415>.